Journal of Physics: Conference Series

PAPER • **OPEN ACCESS**

Adaptive bionic joint base on the flexibility feature of ostrich intertarsal joint

To cite this article: R Zhang *et al* 2020 *J. Phys.: Conf. Ser.* **1507** 052007

Journal of Physics: Conference Series **1507** (2020) 052007 doi:10.1088/1742-6596/1507/5/052007

Adaptive bionic joint base on the flexibility feature of ostrich intertarsal joint

R Zhang[1], Q Q Cao[1], L Ling[1], L X Kong[1], C Wang[1], B Su[2], L G Wen[3] and J Q Li[1]

[1]Key Laboratory of Bionic Engineering, Ministry of Education, Jilin University, Changchun 130022, P.R. China;
[2]China North Vehicle Research Institute, Beijing 100000, P.R. China;
[3]School of Mechanical and Aerospace Engineering, Jilin University, Changchun 130022, P.R. China.

E-mail: wen-lg@126.com

Abstract. The joints of traditional foot robots are generally designed as power-driven articulated rotary motion, but this design has some problems such as poor flexibility and adaptability. To optimize joints, this paper selected the African ostrich intertarsal joint which could move at high speed in complex terrain as a biomimetic prototype. Based on the motion acquisition and reverse engineering three-dimensional reconstruction of the intertarsal joint, a rope-driven spherical sub-bionic joint was designed. The angle curves of the bionic joints under different ground conditions were obtained through the hard ground and the motion tests of three different softness sands (medium with different particle sizes). Results showed that the proportion of the vacant period was 35%, 49%, 62% and 63% when the bionic joint moved on the hard ground and three soft grounds (the particle size particles are arranged from large to small),. The range of variation gradually becomes larger, similar to the variation trend of the intertarsal joint during ostrich locomotion. The bionic joint was able to absorb joint impact through the relative slippage of the joint surface and expansion/contraction of the rope, and maintain flexibility when passing through different degrees of softness.

1. Introduction

Foot-based robots are becoming more and more complicated due to their good adaptability to soft and hard ground. However, foot robots have discrete gait characteristics, which cause the body to collide with the ground continuously, making the joint movement non-compliant. At present, most foot robots simplify the muscle and tendon-driven spherical sub-joints into electric motors and hydraulically driven articulated joints. Due to the obvious difference in joint stiffness between the vacating period and the swinging period, the ground reaction force at the moment of touching the ground will have a greater impact on the joint. The impact load will also deviate from the sagittal plane due to the uncertainty of the ground environment and the attitude of the ground contact. where the 2D plane is located.

Therefore, simplifying the joint into an articulated rotational motion reduces the flexibility of the joint, causing problems such as joint wear and body instability. Domestic and foreign scholars usually use the machine electric hydraulic system and variable stiffness adaptive control design method to solve the discrete gait and maintain the flexibility of the joint. The Cassie robot acquires the real-time state of the joint through the position sensor at each joint, thereby improving the robustness during walking [1]. The BigDog robot generates a gait coordination algorithm through the three-dimensional force sensor of the leg through the processor to generate a gait coordination algorithm, and then feeds back to the leg to achieve a sTable gait [2, 3]. HyQ is equipped with a hydraulic servo system and control system at the joints of the legs. It is controlled by hydraulic and motor hybrid drive to achieve a variety of gait movements [4-6]. Cheetah is directly driven by the motor through the small reduction ratio reducer at the joint to directly control the joint torque through the motor current to maintain the stability of walking [7-9]. The DURUS robot uses an energy-efficient deceleration mechanism to directly control the torque of the leg joints through a torque motor, while optimizing the gait [10]. Some research institutes in China developed four-legged robot used hydraulic or hydraulic driving at the joints, which is characterized by fast response and high precision [11-32].

In addition, the variable stiffness adaptive method has certain help to the discrete gait. A cam disc roller variable stiffness joint with compact structure, high energy density and high robustness was designed. The variable stiffness joint adjusts the position of the stiffness motor to adjust the preload of the floating spring and the relative position of the cam disc roller structure to achieve joint stiffness variation [33, 34]. A variable stiffness joint that automatically adjusts the pre-tightening stiffness of the joint by combining an axially floating spring unit with a free system called BLAPS was designed [35]. A variable stiffness drive actuator based on a four-bar mechanism was designed. The device is composed of a ring inner ring frame and an outer ring frame and a deformed elastic element. The outer ring is rigidly connected with the output link. The inner ring is rigidly connected with the input shaft. The variable stiffness elastic element is actually a hinged joint for a small connection with a deformed four-bar mechanism. Joint stiffness and position can be independently controlled. The structure is very compact, small in size, easy to assemble and robot joints [36]. A new type of nonlinear elastic actuator (ANLES) was proposed using a torsion spring wound around a guide bar with a curved profile to produce a nonlinear relationship between angle and torque [37]. A variable stiffness device using a planar prismatic torsion spring was designed. The device is pre-tensioned by a polygonal torsion spring to change the rigidity of the device, and has a large rigidity adjustment range and a compact structure [38]. Machine electrical hydraulic system and variable stiffness adaptive control design can improve collision safety, but the way to improve joint performance is often accompanied by complex control strategies and structural design [39].

After a long period of natural evolution, the organism has a perfect physiological structure and movement mechanism, which can adapt well to the complex and changing natural environment. Inspired by nature, it has always been the dream of engineers to develop a soft, safe and efficient bionic joint that rivals biological biology through research on biological joints [39].

The African ostrich has excellent athletic ability and is the largest biped in the world with the fastest weight [40,41]. The ostrich's intertarsal joint is located in the middle of the leg. There is no muscle wrap around the joint, it relies solely on the flexor and extensor tendons to provide power, and the medial and lateral ligaments and joint surfaces provide stability. This special biostructure assembly can satisfy the high speed and maneuvering motor function of the ostrich [42]. Rubenson J et al. combined with gross anatomy to establish a 5-segment 17-degree-of-freedom kinematics model of the ostrich hind limbs, and determined that the rotational axis of the intertarsal joint was rotated 21° relative to the sagittal plane for non-sagittal motion [43]. Schaller N U et al. found that the ostrich intertarsal joint interacted with the joint surface of the ligament. When the joint crossed about 115°, the joint would rapidly expand and contract, and the passive rebound mechanism could save exercise energy [44]. At present, the research on bionic joints mostly through the abstract extraction of physiological structure, often lack of combination with joint motion analysis. Therefore, based on the motion parameters and physiological structure of the ostrich intertarsal joint, combined with the excellent movement and adaptation characteristics of the joint in different ground environments, a rope-driven adaptive bionic joint with flexible characteristics is designed by engineering bionics.

2. Materials and method

2.1. Ostrich intertarsal joint kinematics

2.1.1. Experimental object and device. The study was an 8-month-old Asian adult female ostrich with a height of about 180 cm and a body weight of about 83 kg. It was from a large ostrich farm in Ji'an, Jilin Province of China. The ostrich was selected as a test object for the study of ostrich movement mechanism. In order to ensure that the ostrich adapts to the test site and obeys the tester's instructions, the ostrich is trained for half a month before the start of the test, and the soft ground and hard ground sports training is performed every morning and afternoon. Perform 20 round-trip runs with appropriate rest and eating in the middle. The field test equipment is shown in table 1.

Table 1. Field test equipment.

Name	Function
Three high speed cameras (CASIO EX-FH25)	Simultaneous video
3d calibration framework	Calibration of test site
Mark points	Marks a specific point in the location to be studied
Flash (JY181B)	Sync release
Light source (FCCE)	Add light intensity
RSscan International Pressure plate （2.096 m*0.472 m*0.025 m）	Plantar pressure collection

2.1.2. Regression equation Acquisition process. Set up the collection area (1.4 m * 4 m), the upper part is covered with a black shade net to avoid daytime test under strong light. There are 38 meters long and 2 meters wide running and rest areas on both sides. The three areas have a 1.5 m high fence. The non-slip rubber is arranged above the pressure plate, the marble plate is arranged below, and the pressure plate is embedded in the hard ground. The specific test site layout is shown in figure 1.

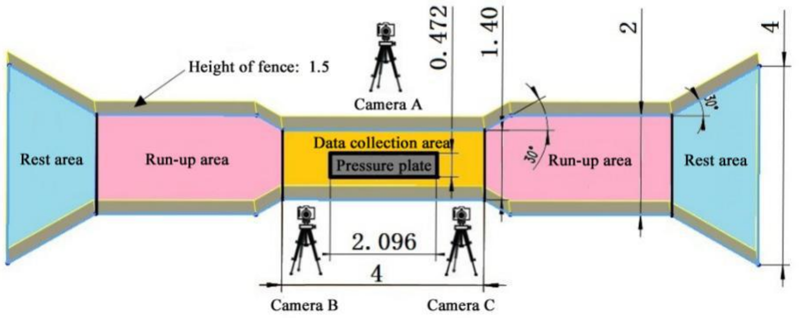

Figure 1. Experimental field layout.

The marker points are attached to the distal tibiotarsus of the right foot of the ostrich, the proximal tarsometatarsus and the intertarsal joint, as shown in figure 2. Set the camera sampling frequency to 120 fps uniformly. The calibration frame is placed in the middle of the pressure plate and the space coordinate system is calibrated. Drive the ostrich at different speeds so that the ostrich passes straight through the test collection area while walking or running. When the ostrich moves to the vicinity of the test collection area, turn on the flash to give a high-brightness exposure moment in the camera's view. Among them, when measuring the movement data of the ostrich on the soft ground, the loose sand with a height of 0.04 m is evenly arranged above the non-slip rubber. The pressure plate is calibrated before each test to ensure accurate data. After each data sampling is finished, check whether all data is abnormal. If there is an abnormality, the test is restarted.

Figure 2. Location of leg marker.

2.2. Design of bionic joint system

Taking the intertarsal joint as a biomimetic prototype, based on the engineering bionic technique, the medical image data of the intertarsal joint model was extracted from the nuclear magnetic scan image (CT) of the ostrich by the medical image control system software, and the intertarsal joint was used by the reverse engineering software. After the operation of noise reduction, smoothing, etc., a three-dimensional model of the intertarsal joint was obtained. Based on this, a three-dimensional mapping software was used to design the rope-driven bionic joint. The bionic joint is mainly divided into two parts: the spherical sub-engagement joint, Bionic joint drive system.

2.2.1. Design of spherical pair engaged joint. Based on the existing study on the general anatomy of the intertarsal joint of ostrich [44], the lateral articular fossa of the tarsometatarsus lateral joint and the lateral tarsometatarsus metatarsal bone were parallel to the sagittal plane, the medial tibiotarsus articular head and tarsal metatarsal medial articular fossa presented an angle of 15° medial to the sagittal plane, and the joints exhibited non-sagittal motion. At the same time, triangular sesamoid bone is present in the posterior tibiotarsus, which prevents hyperextension of the joint. In addition, there is cartilage tissue on the bone surface of the ostrich intertarsal joint, which can absorb impact through deformation, and maintain the joint flexibility when the ostrich intertarsal joint moves, in accordance with the cooperative system formed by fascia, medial and lateral ligaments and anterior and posterior ligaments at the joint, as shown in figure 3b.

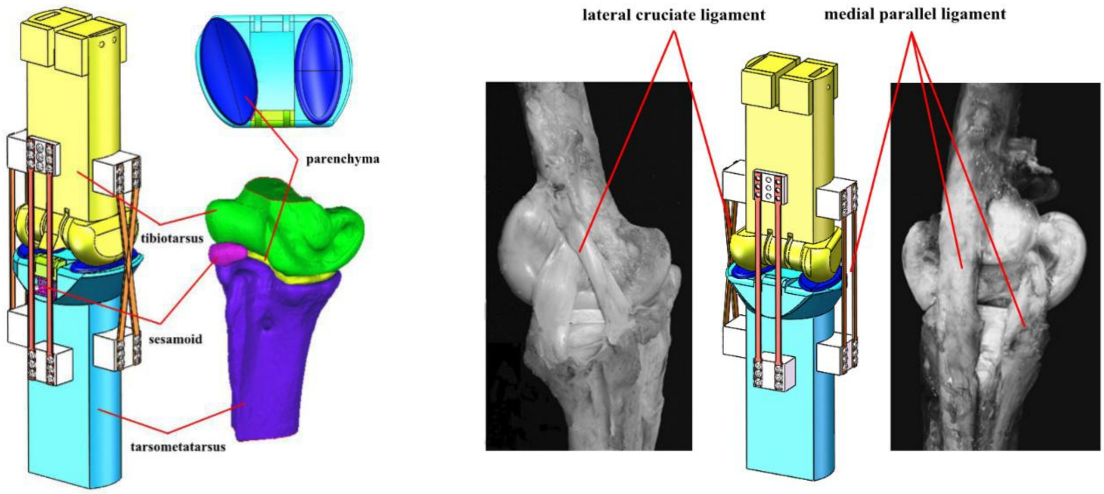

a. Comparison between the rigid parts of the bionic joint and those of the intertarsal joint in ostrich.

b. Comparison between the flexible parts of the bionic joint and those of intertarsal joint in ostrich [44].

Figure 3. Bionic joint based on ostrich tarsal joint.

The internal joint head and the internal socket of the bionic joint are at an angle of 15° to the sagittal plane of the joint by bionic engineering. There is a cushion between the joint head and the socket to simulate soft tissue action. There is a double spring cushion seat at the joint of the lower rod, together with the cushioning slider, and a triangular sesamoid model with a ratcheting simulation at the rear end of the joint head of the upper rod constitutes a synergistic system to prevent the joint from overstretching, as shown in figure 3a.

2.2.2. Drive system. The tendon drive of the ostrich intertarsal joint is simplified to the rope drive under the motor. Since the rope can only withstand the tension and can not withstand the pressure, the rope-driven robot must be driven by redundancy, that is, at least n+1 ropes can be used to drive n degrees of freedom [45]. In order to achieve rotational freedom in the sagittal plane, it is necessary to cooperate with the two drive units of the curved rope and the extension cord. At the same time, the joint rotation angle must correspond to the motor rotation angle.

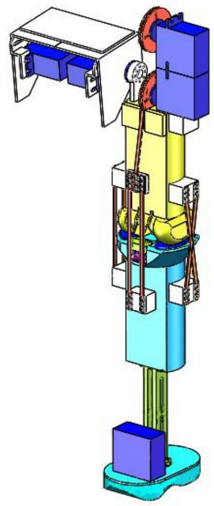

a. 3d model with drive system.

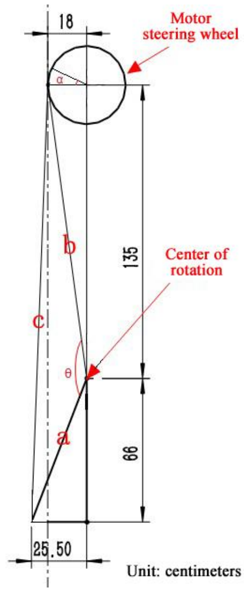

b. Joint driven simplified model.

Figure 4. Joint driven model.

As shown in figure 4a, A 3d model of the rope drive of joints can be obtained by simplifying the driving simplified model in figure 4b. In the simplified model, a, b are the calculated torso lengths and c is the length of the drive rope. As can be seen from the figure 4b, the arc length of the steering wheel rotation is equal to the length of the rope change. Combine the cosine formula and the arc length formula to get the formula 1.

$$\sqrt{a^2+b^2\text{-}2ab\cos\theta_2}\text{-}\sqrt{a^2+b^2\text{-}2ab\cos\theta_1}=r\cdot\Delta\alpha \tag{1}$$

Where,
θ_2 is the angle of the joint after the change,
θ_1 is the angle of the joint before the change,
$\Delta\alpha$ is the angle at which the motor steering wheel changes,
θ、α is radians.
The size of the graphic can be obtained by substituting,

$$\sqrt{23590\text{-}19339.6\cos\theta_2}\text{-}\sqrt{23590\text{-}19339.6\cos\theta_1}=18\cdot\Delta\alpha \tag{2}$$

Let x=cosθ，y=α can get the equation,

$$\Delta y=\frac{1}{18}\cdot(\sqrt{23590\text{-}19339.6x_2}\text{-}\sqrt{23590\text{-}19339.6x_1}) \tag{3}$$

Obtain an equation by indefinite integral of y and x,

$$y=\frac{1}{522169.2}\cdot(23590\text{-}19339.6x)^{\frac{3}{2}}+C \tag{4}$$

From the initial condition x=0.872159，y=0 gives C=-0.07747. At the same time, y=α、x=cosθ are substituted into the equation, and finally the relationship between the joint angle and the angle of rotation of the motor can be obtained.

$$\alpha=\frac{1}{522169.2}\cdot(23590\text{-}19339.6\cos\theta)^{\frac{3}{2}}\text{-}0.07747 \tag{5}$$

2.3. *Design of bionic joint system*
Three mediums with different particle sizes were selected as the soft ground environment for the test, and the bottom of the test bench was used as a hard ground environment. Place the bionic joint on the test bench for exercise testing.

2.3.1. Media mechanicals parameters. The particle size distribution of the medium was quantitatively analyzed by BT-9300ST laser particle size distribution analyzer. The results are shown in figure 5.

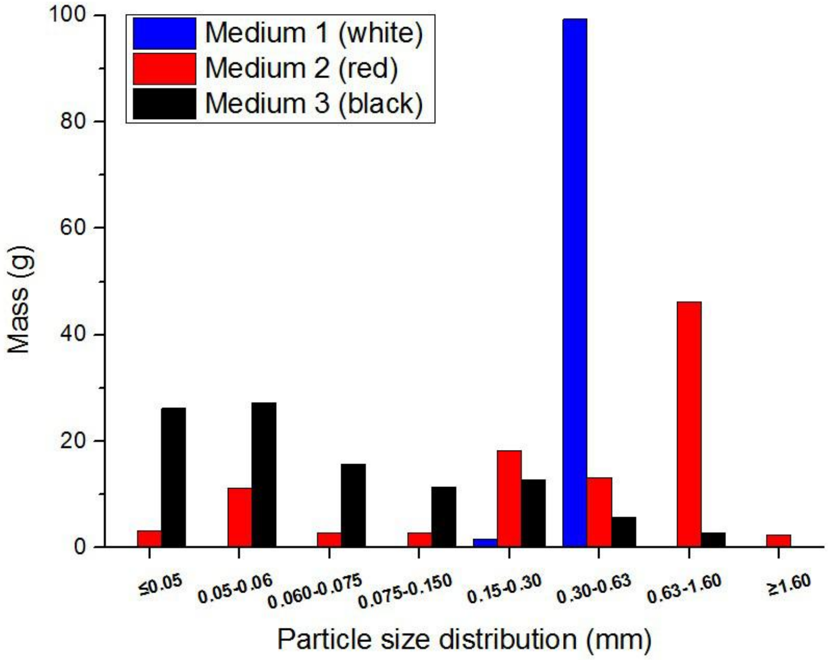

Figure 5. Media particle size distribution.

The particle size of the medium 1 is concentrated at 0.63-1.6 mm, and the particle size is the coarsest, granular, and the medium hardness is the highest. The medium 2 has a particle diameter of 0.63-0.06 mm, and the particle diameter is between the medium 1 and the medium 3 particle diameter, and the particle powder is mixed, and the hardness is second. The medium 3 has a particle size of between 0.15 and 0.06 mm and has the finest particle size and is in the form of a powder. The medium has the lowest hardness.

2.3.2. Experimental equipments. The test bench has a specification of 150 mm*40 mm*40 mm, and has an adjustable height platform on both sides to fix the linear slide (radius 10 mm, length 200 mm). The test background was occluded with a blue cloth, and the motion of the structure was captured by two high-speed cameras. The test site layout is shown in figure 6.

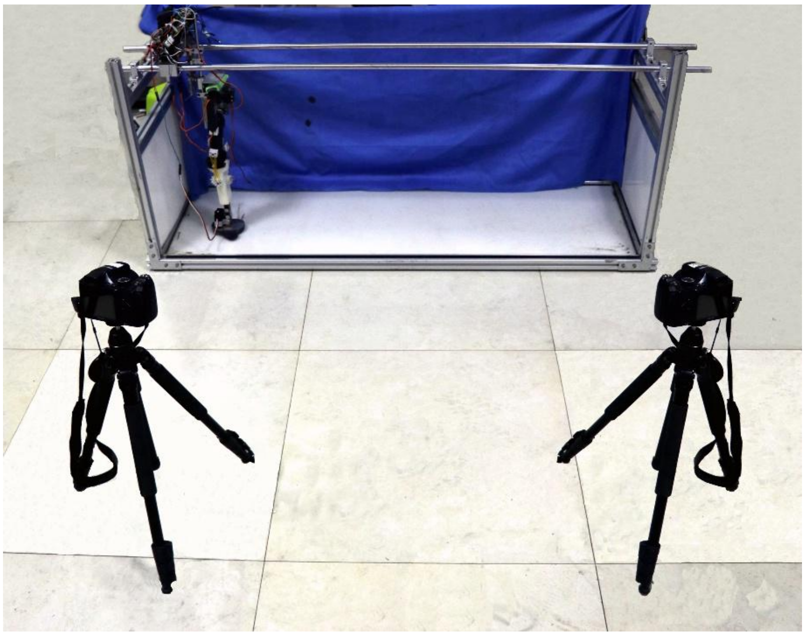

Figure 6. Filed layout.

2.3.3. Steering gear parameters. The motion of the joint adopts the position control method, that is, the adjustment of the joint state is realized by the change of the position at different moments. In order to achieve the timeliness of the joint response and the required torque, the test is to select the DS3218mg dsservo steering gear. The specific parameters of the steering gear are shown in table 2.

Table 2. Specific parameters of dasheng steering gear.

rated voltage	5V	rated current	1.8 A
mass	0.06 kg	Dead zone set	3 ms
size	40*20*47.5 mm	orange line	Single
working temperature	55℃	red line	Vcc
Operating angle range	180°	brown line	Gnd
speed	60°/0.16 s	torque	200 N*cm
rated voltage	5 V	rated current	1.8A

2.3.4. Working condition and process. The test consisted of a structure consisting of a bionic joint through a frame and a linear slide. Mark points 1, 2, and 3 are selected on the joint member, the joint rotation center, and the lower member, as shown in figure 7a, b. The test is divided into four working conditions: the bottom of the test bench is not laid with medium (hard ground environment), and the three media are evenly laid on the bottom of the test bench with the specifications of length, width and height of 50mm*40mm*5mm (three kinds of soft ground environment), from left to right, medium 1, medium 2, and medium 3.

Three successful trials were taken for each condition. Before the start of the working condition test, calibration is carried out through the calibration frame.

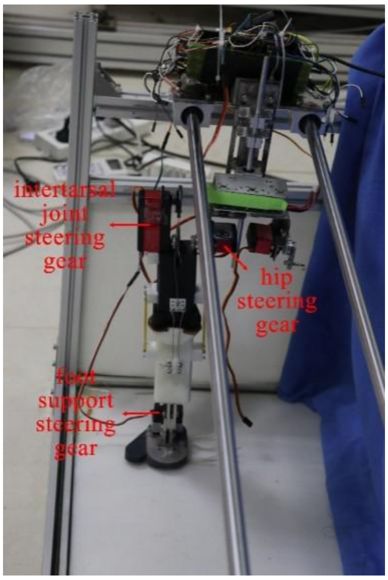

a. Motion drives the steering gear.

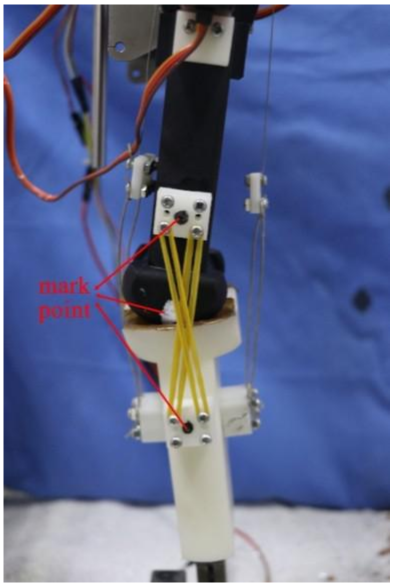

b. Mark point.

Figure 7. Motion-driven steering gear and joint marking points.

3. Result

3.1. Ostrich locomotion experimental results

The two-dimensional/three-dimensional motion image capture system analysis software Simi motion was used to analyze the motion image of a gait cycle of the ostrich's intertarsal joint, the intertarsal joint motion feature points were picked frame by frame, as shown in figure 8.

Figure 8. Motion capture of the intertarsal joint of ostrich.

After obtaining the raw data of the tibiotarsus marker point *S*, the joint marker point *J*, and the tibiotarsus marker point *T* space, the smoothing process is respectively performed, and finally a three-dimensional motion stick diagram of a gait cycle of intertarsal joint is obtained, as shown in figure 9.

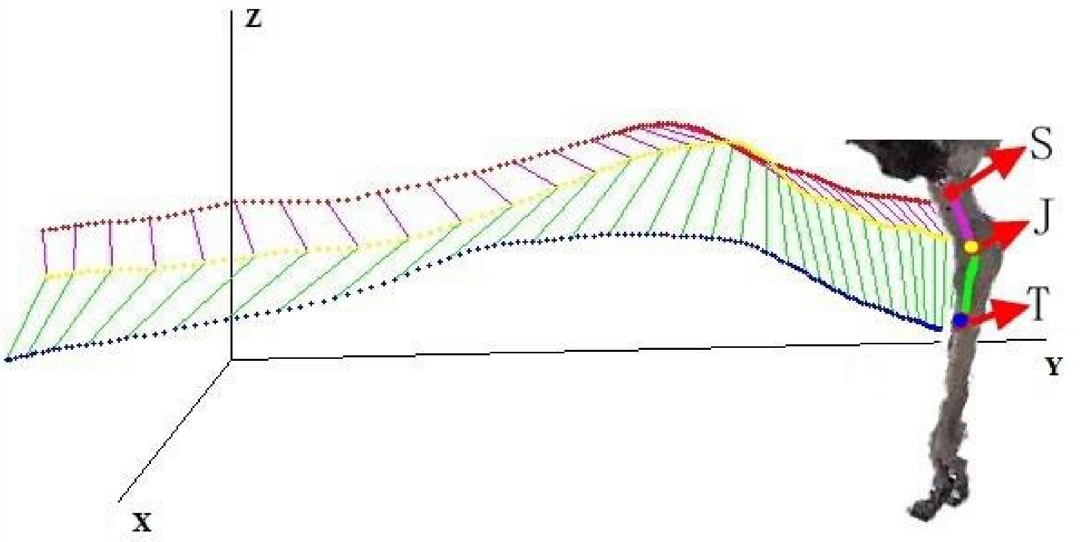

Figure 9. Ostrich skeletal joint movement stick diagram.

The Simi Motion software was used to track the angle of the intertarsal joint in real time, and the joint angle of a gait cycle in the running/walking gait of the soft ground and the hard ground was extracted, and each working condition was recorded three times. The gait cycle is percent, as shown in figure 10.

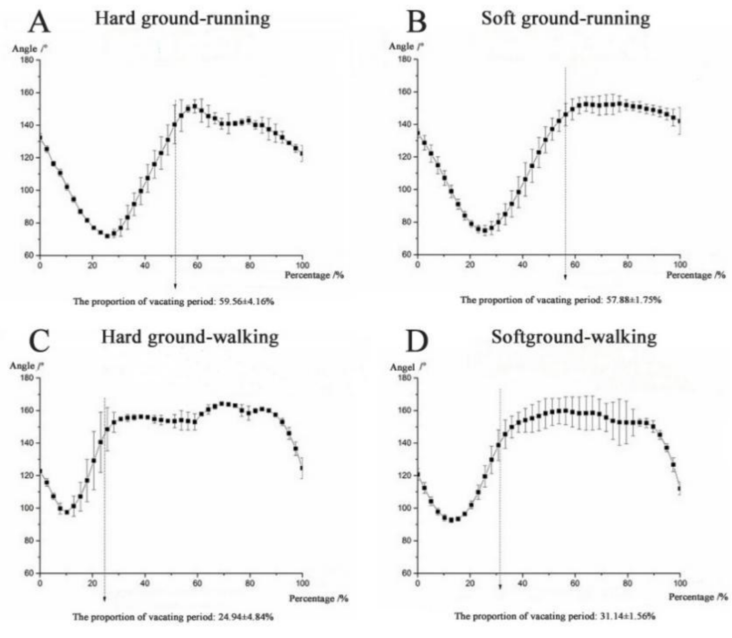

Figure 10. Curve of the angle of the intertarsal joint during the ostrich exercise test (the vacancy is greater than 50% for the running state, and vice versa for the walking gait).

The ostriches took 31.14% and 24.94% of the vacant period when they walked through the soft and hard ground. The percentage of the vacant period when they walked through the soft and hard ground was 57.88% and 51.62%.

3.2. Bionic joint experimental results

Through the high-speed camera system, the joint angle of the joint on the hard ground, medium 1 (white), medium 2 (red), medium 3 (black) is tracked, and the joint angle of the bionic joint can be obtained by Simi Motion software extraction. The curve of variation is shown in figure 11.

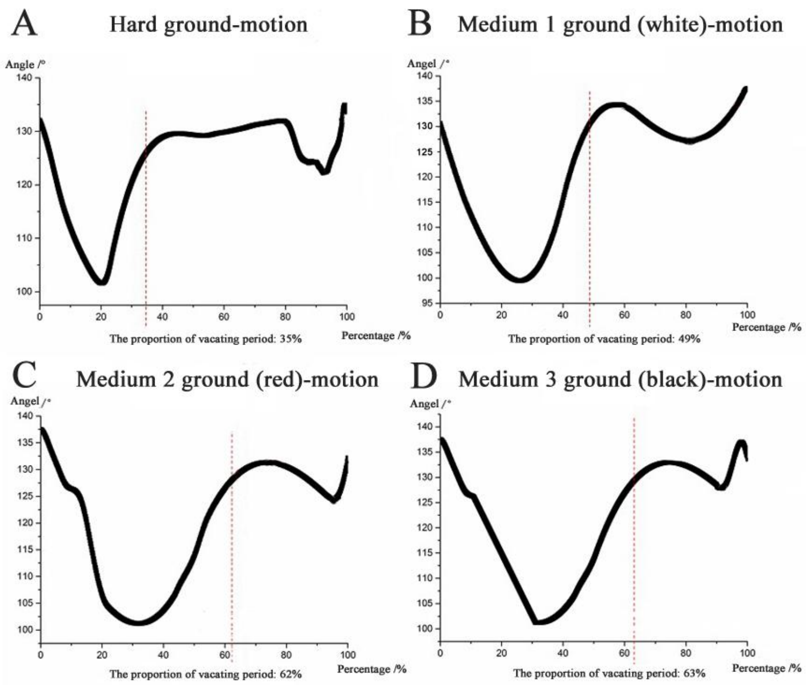

Figure 11. Bionic joint angle curve.

Based on the bionic joint motion test data, the joint angle varies from 100 to 135°, and the joint vacancy period is 35%, 49%, 62%, and 63%, respectively. Correspondingly, the joint angle varies from 121 to 132°, 126-135°, 125-133° and 127-132° during the vacant period.

4. Discussion

Existing studies established a 17-degree-of-freedom kinematics model of 5 segments of ostrich hind limbs and obtained the angle changes of each joint of ostrich at the speed of 3.3m/s, so as to determine the actual rotation center and rotation axis of joint motion, proving that the joint motion of ostrich's metatarsal bone was not limited to two-dimensional plane but three-dimensional [43]. On the one hand, the interaction between the ligaments of the intertarsal joints and the joint surface is equivalent to the "engagement-disengagement" of the motion process. This structure can effectively maintain the stability of the joints and maintain the flexibility of the joint movement through the passive rebound mechanism [44]. On the other hand, flexibility is also reflected in the soft tissue of the tendon and ligament of the anterior and internal and external joints of the joint [42]. Therefore, the abstract extraction of factors such as tendon, ligament and joint morphology is important for the flexibility of joints.

When the ostrich is running, the hard ground has obvious angular fluctuations compared with the soft ground, which is about 9°, the proportion of the patency period of the intertarsal joint increases as the degree of softness of the ground increases. In addition, while the peak of the change in the walking gait is not obvious. We speculat that the ostrich are slower in walking, have smaller stride, and cannot fully flex or extend their joints. Based on the results of bionic joint exercise data, the proportion of joint vacancy period increases with the increase of the degree of softness of the ground, and the range of joint angle also shows an increasing trend. In other words, the greater the ground hardness, the more pronounced the impact on the joint. The bionic joints we designed can maintain flexibility when they pass through different degrees of softness, And there is no significant difference between the trend of the vacant period and the ostrich's exercise test.

The use of rope drive can reduce the moment of inertia, can achieve a large movement space, while occupying a small space, light weight, and play a very good flexibility [45, 46]. In the process of the front and rear squats of the bionic joints driving the bionic joints forward, the ground reaction force forms a torque at the joints to drive the joints to bend, but the front and rear drive ropes are in a tight state to maintain the flexibility of the joints, and maintaining joint stability, combined with a soft ground environment, can cause the entire leg to sink and have a tendency to return the joint to a stretched state. Therefore, the angle of the joint of the soft ground environment in a harder ground environment will be smaller. On the other hand, since the hard ground leg does not sink relative to the center of gravity, the steering gear is required to drive the rope to extend the joint, and the completion of the kicking action of the leg requires the center of gravity of the mechanism to be raised, thus requiring more energy. Therefore, under the condition that the output torque of the joint-driven steering gear is the same, the hard ground has a smaller proportion of the soft ground vacancy period.

Considering the choice of steering gear for bionic joints, this paper only selected a speed. There are still many aspects of work in the future. On the one hand, there is a lack of quantitative analysis of the arrangement of the medial and lateral ligaments of the bionic joints, the stiffness of the elastic elements, and the selection of soft tissue materials for the joint surfaces. On the other hand, the drive rope lacks a tensioning structure, which causes slack after a period of motion and requires further optimization.

5. Conclusion

The adaptive bionic joint base on the flexibility feature of ostrich intertarsal joint refers to biological physiological structure and motion parameters: special mesh morphology, elastic element simulation ligament, and bionic design with buffer pad and sesamoid bone. The combination of structure and motion analysis breaks the traditional joint assembly mode and provides a new idea for joint design optimization of foot robots.

Based on the ostrich exercise test and the biomimetic joint test data, the biomimetic joints can maintain flexibility when passing through the environment of different degree of softness, and there is no obvious difference between the trend of the proportion of flying period and the ostrich exercise test, which verifies the rationality of the biomimetic joint design.

Acknowledgments

This work was supported by the National Natural Science Foundation of China (No. 51675221, 91748211), the Science and Technology Development Planning Project of Jilin Province of China (No. 20180101077JC), the Science and Technology Research Project in the 13th Five-Year Period of

Education Department of Jilin Province (No. JJKH20190134KJ), and the Graduate Innovation Fund of Jilin University (No. 101832018C006).

Reference

[1] Xie Z , Berseth G , Clary P , et al. 2018 *Feedback control for cassie with deep reinforcement learning*
[2] Raibert M , Blankespoor K , Nelson G , et al. 2008 *IFAC Proceedings Volumes* **41**(2) 10822-5
[3] Lianghong D. 2015 *Journal of mechanical engineering* **51**(7) 1-23
[4] Semini, C., et al. 2011 *Journal of Systems and Control Engineering* **225**(6) 831-49
[5] Ugurlu, B., et al. 2013 *Intelligent Robots and Systems* (IROS) 2013 Conference
[6] Semini C, Barasuol V,Goldsmith J , et al. 2016 *IEEE/ASME Transactions on Mechatronics* **99** 1
[7] Rutishauser S, Sprowitz A, Righetti L, et al. 2008 *IEEE Ras&Embs International Conference on Biomedical Robotics and Biomechatronics* pp 710-5
[8] Seok S, Wang A, Chuah M let crl. 2013 *Proceedings of International Conference on Robotics and Automation* pp 3307-12
[9] Reher J, Cousineau E, Hereid A, et al. 2016 *Proce of IEEE International Conference on Robotics and Automation* pp 1794-801
[10] Cai R B, Chen Y Z, Hou W Q, et al. 2013 *International Journal of Advanced Robotioc System* **10** 148
[11] Peihua C, Qixin C, Hongxu M. 2013 *Journal of southeast university* (natural science edition) **43**(z1)
[12] Peihua C, Qixin C. 2013 *Journal of huazhong university of science and technology* (natural science edition) **41**(z1).
[13] Hu N , Li S , Huang D , et al. 2014 Crawling Gait Planning for a Quadruped Robot with High Payload Walking on Irregular Terrain.
[14] Liming D. 2014 *Design and research of real - time control system for quadruped elephant robot* Shanghai jiaotong university,
[15] Xian B and Feng G 2013 Design of spring parameters of new hydraulic quadruped robot// Shanghai Jiaotong University Doctoral Academic Forum - Mechanical Centennial Intelligent Manufacturing Intelligence China Academic Forum.
[16] Xing H and Feng G 2013 Four-legged robot foot force identification method using distributed sensor system// Shanghai Jiaotong University Doctoral Academic Forum - Mechanical Centennial Intelligent Manufacturing Intelligence China Academic Forum.
[17] Liming D, Xianchao Z and Chenkun Q 2014 *Research on real-time control system of open walking robot*. Mechanical design and research, (3).
[18] Chai H, Meng J, Rong X, et al. 2014 Design and implementation of SCalf, an advanced hydraulic quadruped robot. *Robot*.
[19] Hui C, Jian M and Xuewen R 2014 *Robot* **36**(4) 385-91
[20] Li B , Li Y , Rong X , et al. 2013 *The Effects of Leg Configurations on Trotting Quadruped Robot China Intelligent Automation Conference*
[21] Jian M 2015 Research and implementation of motion control method for quadruped robot in complex terrain environment Shandong University
[22] Jian M, Yibin L and Hui C 2015 *Robot* **37**(1) 85-93
[23] Guoteng Z, Xuewen R and Yibin L 2016 *Robot* **38**(1) 64-74
[24] Li M , Jiang Z , Wang P , et al. 2014 *Journal of Bionic Engineering* **11**(2) 188-98
[25] Mantian L, Zhenyu J and Pengfei W 2015*Journal of Jilin University (Engineering and Technology Edition)* **45** 5
[26] Mantian L, Zhenyu J and Wei G 2014 *Robot* **36**(1) 21-8
[27] Yiqun L, Zongquan D and Zhen L 2015 *Journal of Mechanical Engineering* **3** 10-7
[28] Junyao G , Xingguang D , Qiang H , et al. 2013 The research of hydraulic quadruped bionic

robot design *Complex Medical Engineering (CME)* 2013 ICME International Conference on IEEE pp 620-5

[29] Lipeng W, Junzheng W and Shoukun W 2013 *Journal of Mechanical Engineering* **49**(1) 39-44

[30] Baoling H, Huanfei L and Qingsheng L 2014 *Computer measurement and control* **4** 1163-5

[31] Siyu C 2014 *Research on structural design of quadruped bionic robot* Huazhong University of Science and Technology

[32] Wolf S , Eiberger O , Hirzinger G , et al 2011 The DLR FSJ: energy based design of a variable stiffness joint *IEEE International Conference on Robotics & Automation*

[33] Wolf S , Hirzinger G .2008 *IEEE International Conference on Robotics and Automation* 1741-6

[34] Torrealba R R , Udelman S B , Fonseca-Rojas E D , et al 2017 *Mechanism and Machine Theory* **116** 248-61

[35] Gianluca Palli, Berselli, Melchiorri and Gabriele Vassura 2011 *Journal of Mechanisms and Robotics* pp 1-5

[36] Koichi Koganezawva 2005 *Proceedings of the 2005 IEEE/RSJ International Conference on Intelligent Robots and Systems* 2005 pp 1544-51

[37] Abin L, Jianjun Z and Yaping Z 2013 *Mechanical and electrical engineering* **30**(4) 439-43

[38] Dunwen W, Wenjie G and Tao G 2017 *Robot* **39**(4) 541-50

[39] Rui Z, Sihua Z and Fang L 2011 *Analysis of the mechanism of ostrich sand movement*. Proceedings of the 2011 Annual Conference of the Chinese Society of Agricultural Engineering

[40] Schaller N U, Herkner B, Prinzinger R, et al. 2005 Locomotor characteristics of the ostrich (Struthio camelus) I: Morphometric and morphological analyses

[41] Rubenson J, Lloyd D G, Besier T F, et al. 2007 *Journal of Experimental Biology* **210**(14) 2548-62

[42] Rubenson J , Lloyd D G , Heliams D B , et al. 2011 *Journal of the Royal Society Interface* **8**(58) 740

[43] Schaller N U, Herkner B, Villa R, et al. 2010 *Journal of Anatomy* **214**(6) 830-47

[44] Xiufeng S, Sun C, Bai C, et al. 2014 *Application technology* **41**(4) 51-5

[45] Conghao W, Chun Z, Jiayi L, et al. 2018 *Mechanical Engineers* **323**(05) 19